ORIGINAL PAPER

CrossMark

Fatigue–creep interaction based on continuum damage mechanics for AISI H13 hot work tool steel at elevated temperatures

Hai-sheng Chen[1] · Yong-qin Wang[1,2] · Wei-qi Du[1] · Liang Wu[3] · Yuan-xin Luo[1,2]

Abstract
AISI H13 (4Cr5MoSiV1) is one of the commonly used materials for extrusion tool, and it suffers from fatigue–creep damage during the hot extrusion process. Stress-controlled fatigue and creep–fatigue interaction tests were carried out at 500 °C to investigate its damage evolution. The accumulated plastic strain was selected to define the damage variable due to its clear physical meaning. A new fatigue–creep interaction damage model was proposed on the basis of continuum damage mechanics. A new equivalent impulse density for fatigue–creep tests was proposed to incorporate the holding time effect by transforming creep impulse density into fatigue impulse density. The experimental results indicated that the damage model is able to describe the damage evolution under these working conditions.

Keywords AISI H13 hot work tool steel · Fatigue–creep · Damage evolution · Continuum damage mechanics · Nonlinear interaction · Damage exponent

1 Introduction

Extrusion is a technique that deforms the material into products with a desired cross-sectional profile. It has a widespread application in industries because the materials extruded can be produced into some very complex cross sections through a die of the desired design. As the most common extrusion material, aluminum can be either hot- or cold-extruded. The hot extrusion process is easier than that of cold extrusion because the extrusion temperature is above the recrystallization temperature of materials and the workpiece can be kept from work hardening [1]. The greatest defect of this process is its large cost for upkeep and replacement of extrusion tools.

To reduce the manufacturing cost and prolong the die life span, it is necessary to understand the failure

✉ Wei-qi Du
cqudwq@outlook.com

1   College of Mechanical Engineering, Chongqing University, Chongqing 400044, China

2   State Key Laboratory of Mechanical Transmission, Chongqing University, Chongqing 400044, China

3   Chongqing Research Institute of China Coal Technology and Engineering Group Corp, Chongqing 400016, China

mechanisms of extrusion dies. Previous investigations considered that wear, fracture and plastic deformation are the most common failure mechanisms of aluminum hot extrusion [2, 3]. However, Reggiani et al. [4] found that creep and low-cycle fatigue may occur simultaneously in the hot extrusion. The load during a typical direct extrusion stroke can be divided into three components: (1) frictional load, which is used to overcome frictional stresses on internal surface; (2) forming load, which is for material flowing; and (3) the third part is to resist the internal deformation work [5]. The forming load bears the main responsibility for exerting stress on the die, and it can be considered stable along the stroke (dwell part of fatigue–creep). On the other hand, multiple billets are extruded sequentially in practical engineering, which leads to the extrusion dies suffering from cyclic load (low-cycle fatigue regime of fatigue–creep). In particular, the temperature is elevated to 450–500 °C for hot extrusion of aluminum, and it will be kept fairly stable during the whole manufacturing process [6]. Therefore, the fatigue–creep interaction is a failure mechanism that should also be taken into considerations in hot extrusion die of aluminum.

AISI H13 (4Cr5MoSiV1) is one of commonly used hot work tool steels for aluminum extrusion dies. The excellent mechanical properties at elevated temperatures, such as

high hardness, high wear resistance and thermo-cyclic stability, make it qualified for hot extrusion dies. Some literatures have investigated the failure mechanisms of AISI H13. Many researches were focused on wear mechanism of AISI H13, and some techniques were aimed at how to improve the high-temperature wear resistance of material [7–9]. Besides, Kchaou et al. [10] investigated a case study of brass gas valves and emphasized the fatigue damage role in the whole complex failure mode. Li et al. [11] paid attention to the mechanism of thermal fatigue crack initiation and propagation of AISI H13. Laser surface remelting, as a new rising technique of surface treatment, was found to be helpful to improve the tensile strength and fatigue resistance of AISI H13 at both room and elevated temperatures [12, 13]. Although AISI H13 is not a new material and it has received a relatively comprehensive study, its nonlinear fatigue–creep interaction during the hot extrusion process still lacks enough concerns.

It is very difficult to precisely describe the damage evolution of fatigue–creep interaction. Although linear damage accumulation (LDA) theory is simple enough and close to reality to some extent, this well-studied method does not have a physical exploration but a phenomenological basis. Therefore, continuum damage mechanics (CDM), which has a stronger theoretical foundation and is a better method than LDA, was proposed in the past decades [14, 15]. In present study, a CDM-based creep–fatigue interaction damage evolution of the AISI H13 steel was proposed and it was identified by stress-controlled creep–fatigue interaction experiments. A novel equivalent fatigue impulse density was proposed by transforming creep impulse density into fatigue impulse density. To study its properties, fatigue and fatigue–creep tests of AISI H13 were performed at 500 °C, which was close to working condition. The accumulated plastic strain was selected to define the damage variable due to its clear physical meaning. Damage exponent was utilized to describe the damage level of material and the effects of mechanical load and holding time.

2 Experimental setup and material

The experimental setup and the tested material can be seen in Ref. [16]. To be specific, the round bar specimens were employed in this study and were tested by an MTS 100-kN fatigue testing machine with a furnace (MTS Furnace 653). The detailed dimensions of specimen and the experiment platform built are shown in Fig. 1. The heating process of all the specimens was controlled the same by computer with 15 min ramping time and 30 min soaking time. The strains during the tests were captured by a ceramic bar with 12.0 mm gauge length.
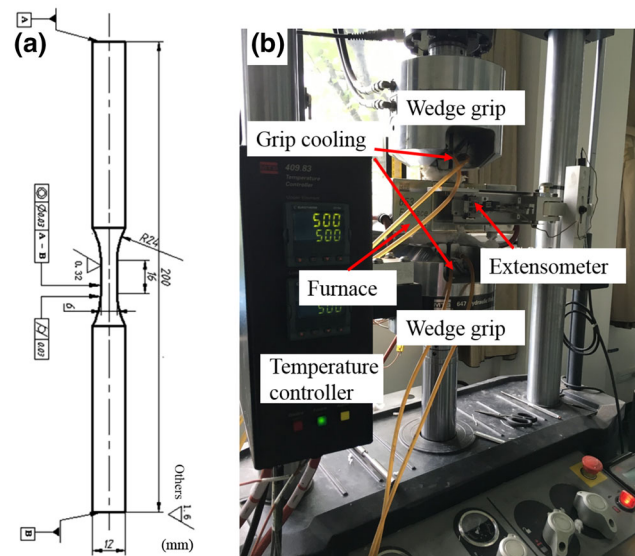

Fig. 1 Test setup. **a** Dimension of test specimen; **b** experimental device settings

The detailed chemical composition (wt%) of employed material AISI H13 is C 0.4, Si 0.97, Mn 0.3, Cr 5.37, Mo 1.34 and V 1.22. Certainly, superior mechanical properties are depending on the heat treatments. The adopted heat treatment is as follows: austenitising for 1 h at 1020 °C, then nitrogen quenching, and then the tow tempering performed twice at 550 and 560 °C, respectively. The micrographs of AISI H13 with different magnifications are presented in Fig. 2 by optical microscope (OM, Olympus measuring laser microscope OLS4000) and JEOL JSM-7800F field emission gun scanning electron microscope (SEM). And the excellent macromechanical properties can also be found by a tensile test, as shown in Fig. 3. Table 1 gives the results of tensile tests at 500 °C for AISI H13 steel.

3 CDM theoretical model for creep–fatigue interaction

CDM can be considered as an effective method to investigate fatigue damage evolution. It describes that the damage of fatigue which is mainly caused by the accumulated plastic strain can be described by an appropriate equation of dissipation potential. The damage evolution of low-cycle fatigue has been proposed by Krajcinovic and Lemaitre [17], and it can be expressed as follows:

$$\dot{D}_f = \frac{\partial \psi}{\partial Y} \tag{1}$$

where $\dot{D}_f$ is the rate of fatigue damage; ψ is dissipate potential; and Y is damage strain energy release rate. There have been various dissipation potential functions until now,
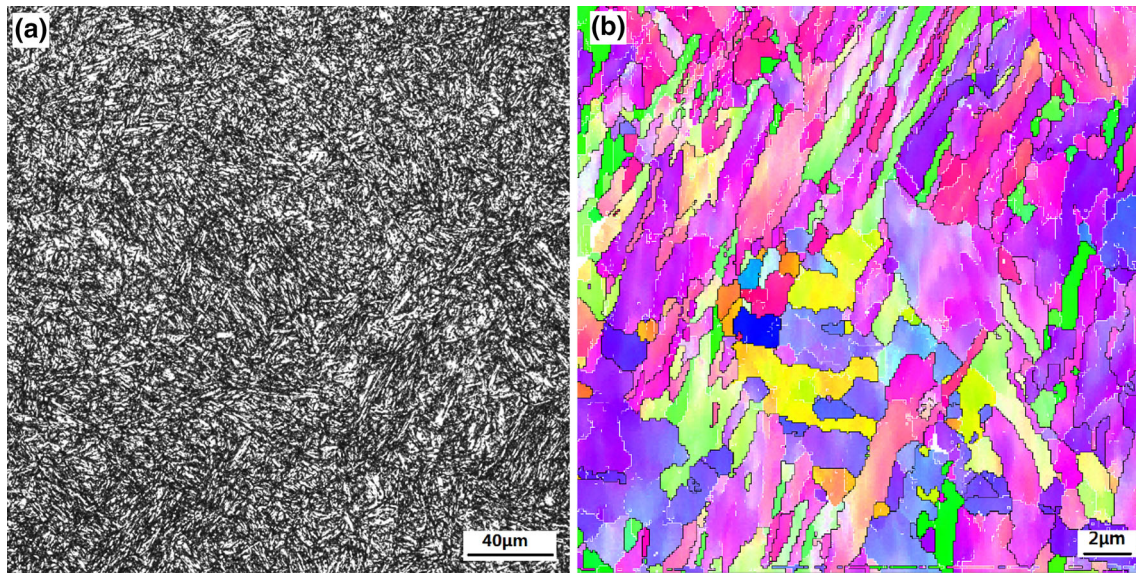
Fig. 2 Different magnitude micrographs after heat treatment. **a** Optical micrograph; **b** electron backscattered diffraction micrograph
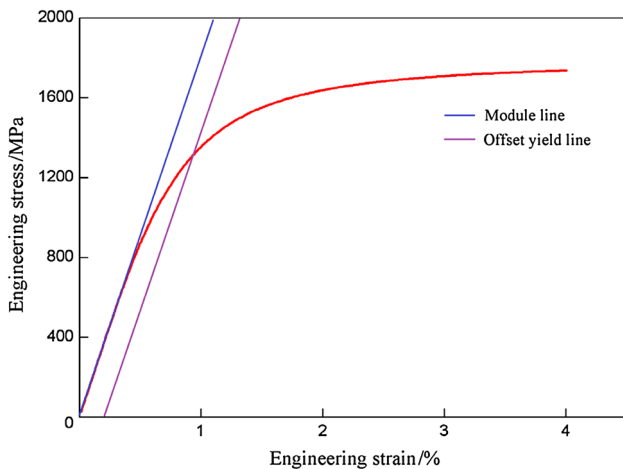

Fig. 3 Stress–strain tensile curve of AISI H13 steel at 500 °C

Table 1 Basic mechanical properties of AISI H13 steel at 500 °C (MPa)

Modulus	Stress at (0.2%) offset yield	Stress at yield
172,184	1330	1749

and the damage potential function proposed by Yang et al. [18] is a most popular one, and it can describe the main properties sufficiently under isotropy:

$$\psi = \frac{Y^2}{2S_0}\frac{\Delta p}{(1-D)^{\alpha_0}} \tag{2}$$

where D is the amount of damage; Δp is the accumulated plastic strain; S_0 is temperature-dependent material

constant which can be obtained by Mason–Coffin relationship; and α_0 is a material constant related to the temperature, loading levels, material properties, etc., which can describe the extent of accumulated damage. Also, Yang et al. [18] considered it more appropriate to reflect the influence of accumulated plastic strain by replacing $(1 - D)$ with $(1 - N/N_f)$, where N is the number of cycles to produce an amount of damage D and N_f is the number of cycles to produce fatigue crack resulting in failure. Thus, the equation can be converted to:

$$\psi = \frac{Y^2}{2S_0}\frac{\Delta p}{(1-N/N_f)^{\alpha_0}} \tag{3}$$

Substituting Eq. (3) into Eq. (1), the obtained isothermal low-cycle fatigue (LCF) damage function can be shown as:

$$\dot{D}_f = \left(-\frac{Y}{S_0}\right)\frac{\Delta p}{(1-N/N_f)^{\alpha_0}} \tag{4}$$

For boundary conditions, $D|_{N=N_0} = D_0$ and $D|_{N=N_f} = 1$, the damage evolution for LCF finally is deduced to:

$$D_f = 1 - (1 - D_0)(1 - N/N_f)^{1-\alpha_0} \tag{5}$$

In the above expression, the damage exponent $1 - \alpha_0$ can be considered as a function of stress for isothermal LCF, in which the damage rate is only dependent on the loading levels. Studies [19, 20] show that the lifetime is significantly related to the stress amplitude recognized as the most important parameter for stress-controlled fatigue. Meanwhile, it is found that the progressive accumulation of plastic deformation induced by tensile mean stress has impact on fatigue life of various materials [21–23]. Therefore, there are many models, such as Goodman [24]

and Smith–Watson–Topper (SWT) [25], which describe the equivalent stress with stress amplitude and mean stress.

In creep–fatigue tests, a tensile dwell time is introduced and the damage mechanism should be considered as time-dependent damage factor to accurately reflect the material behavior. The linear damage summation method was proposed without consideration of the interaction between fatigue damage and creep damage, that is:

$$D_t = D_f + D_c \tag{6}$$

where D_t and D_c represent the total damage and creep damage, respectively.

To understand the fatigue–creep interaction, the fracture surfaces of creep as well as fatigue with different dwell time (0, 10, and 600 s) are observed by SEM. Figure 4a is a typical intergranular brittle fracture graph of creep specimen. The strain localization and cavitation formed at grain boundaries are the main cause of creep failure. The strength of grain boundaries will deteriorate and the grain boundaries become brittle during the creep period. Finally, it leads to the separation of grain boundaries and nucleation of void. It can be found from Fig. 4b–d that fatigue striations become clearer and the number of secondary cracks increases with the increase of dwell time. This is due to the interaction between fatigue damage and creep damage, i.e., creep damage weakens the grain boundaries.

Some efforts are made to figure out the fatigue–creep interaction damage model. Zhang et al. [26] proposed a general creep–fatigue interaction accumulation law by coupling the damage exponent of fatigue and creep into a
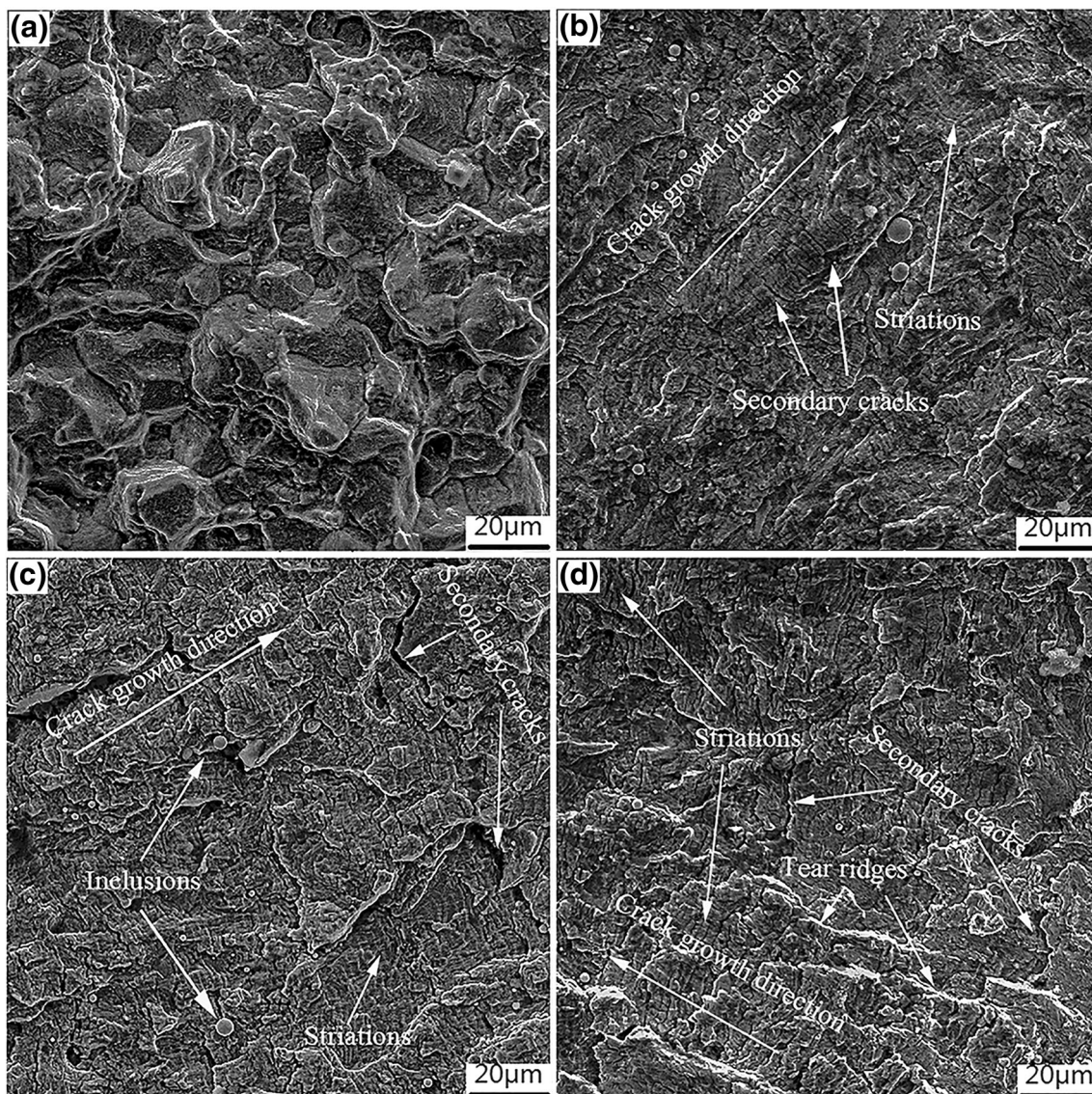

Fig. 4 Fracture micrographs of specimens with different load conditions. a Creep; b fatigue with dwell time of 0 s; c fatigue with dwell time of 10 s; d fatigue with dwell time of 600 s

uniform format. However, stress amplitude was only considered in the damage exponent function for simplification. Fan et al. [14] took mean stress effect into consideration and expressed the damage exponent as a function of maximum stress and stress amplitude. To more precisely describe the damage exponent, an additional time-dependent variable should be introduced. However, variable addition makes the damage exponent become a multivariate function and it is relatively difficult to explore the specific function equation. Hence, it is necessary to search for a novel parameter to combine the effect of stress and holding time similar to the equivalent stress in fatigue process.

The specimen under high-temperature fatigue–creep load will inevitably generate microdefects, such as dislocation, void, and microcrack. Therefore, the internal energy will be changed by these irreversible processes. According to the law of energy conservation, the transformations of energy during the high-temperature fatigue–creep tests can be formulated as [27]:

$$\rho \cdot \frac{\mathrm{d}e}{\mathrm{d}t} = \sigma \cdot \dot{\varepsilon} + \frac{\mathrm{d}Q}{\mathrm{d}t} \tag{7}$$

where ρ is the density of material; e is the internal energy per unit mass; t denotes the time; σ is the applied stress; $\dot{\varepsilon}$ is the strain rate; and Q is the thermal energy. According to Eq. (7), the accumulated internal energy is equal to the sum of external mechanical work and heat exchange. Although the heat transfer is too complex to figure out, it is relevant to the mechanical work for isothermal tests to keep the temperature constant. Hence, the right side of Eq. (7) can be seen as a function of mechanical work:

$$\rho \cdot \frac{\mathrm{d}e}{\mathrm{d}t} = f(\sigma \cdot \dot{\varepsilon}) \tag{8}$$

Since damage generates with the change in internal energy and internal energy is hard to be measured, the function of applied work done can be defined as a parameter to describe material damage. Zhu et al. [28] proposed a novel viscosity-based parameter using stress–time diagram to predict low-cycle fatigue–creep life. The life-predicted model can be widely applicable, and the result showed that it has a good agreement with other reported experimental data. Ji et al. [29] considered that the compression holding period is also deleterious to material and developed a fatigue–creep lifetime model based on applied mechanical work density. The test impulse density E_w was introduced to describe applied mechanical work per cycle, as shown in Fig. 5. It seems more appropriate to be considered as a coupling parameter of stress and holding time. Therefore, the damage exponent could be expressed as a univariate function as follows:
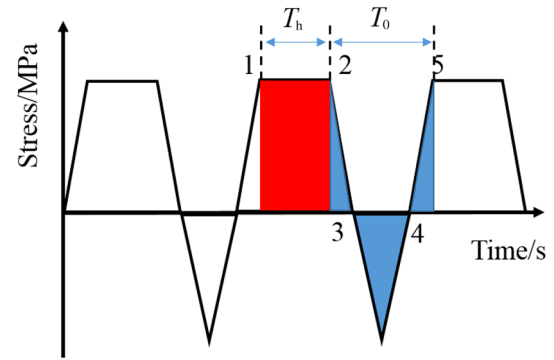

Fig. 5 Stress–time diagram of stress-controlled creep–fatigue test

$$1 - \alpha_0 = f'(E_w) \tag{9}$$

$$E_w = \sigma_{max} \cdot T_h + \frac{(\sigma_{max}^2 + \sigma_{min}^2) \cdot T_0}{\sigma_{max} - \sigma_{min}} \qquad \sigma_{min} \leq 0 \tag{10}$$

$$E_w = \sigma_{max} \cdot T_h + \frac{(\sigma_{max} + \sigma_{min}) \cdot T_0}{2} \qquad \sigma_{min} > 0 \tag{11}$$

where σ_{max} and σ_{min} are the maximum and minimum stresses, respectively; T_0 is the time of variable loading; and T_h denotes the holding time.

However, it can be found in Fig. 4 that the microstructural damage mechanism of creep is relatively different from that of fatigue. More specifically, creep cavitation evolution causes the strain localization near grain boundaries and leads to the void nucleation and propagation, while fatigue cyclic intrusion and extrusion leads to the crack initiation and propagation at the material surface [27]. Therefore, the creep counterpart and fatigue counterpart in impulse density should comply with different energy–damage relationships. Therefore, the applied work done should be divided into two parts, holding time period and the remaining ramp period.

4 Damage parameters and measurement

Generally, damage variable is usually defined as a function of macroparameters since it cannot be measured directly. The definition of damage variable is the key for describing material damage. Several researchers attempted to describe LCF damage by using Yang's modules [30], stable stress range and inelastic strain energy density [23]. For stress-controlled fatigue tests, ratcheting behavior is usually defined as progressive accumulation of plastic strain due to the asymmetrical stress cycling. Ratcheting strain (ε_r) reflects the accumulated plastic strain between the adjacent two hysteresis loops, and it can be mathematically expressed as:

$$\varepsilon_r = \frac{1}{2}(\varepsilon_{min} + \varepsilon_{max}) \tag{12}$$

where ε_{max} is the maximum axial strain and ε_{min} is the minimum axial strain for a particular cycle. Figure 6 shows the ratcheting strain response under the cycle in tension stress of 1600 MPa and compression stress of 800 MPa. It can be found that the rate of ratcheting decays in the initial stage due to cyclic hardening, and then, it maintains a steady state resulting from the balance between cyclic hardening and softening. Finally, the rate of ratcheting suddenly increases and the ratcheting strain reaches a high value until failure. The deformation mechanism is associated with dislocation movement, their interactions and cell formations [31].

It is well known that the ratcheting behavior will deteriorate the mechanical properties of material, and the ratcheting strain can reflect the accumulative effects of fatigue damage [32]. Hence, it is reasonable to define the evolution of ratcheting strain as a damage variable:

$$D_N = \frac{\varepsilon_N - \varepsilon_0}{\varepsilon_f - \varepsilon_0} \tag{13}$$

where D_N denotes the total damage of Nth cycle; ε_N is the ratcheting strain at Nth cycle; ε_0 is ratcheting strain at the first cycle; and ε_f is the ratcheting strain when the specimen reaches failure.

Damage evolution of fatigue–creep can be seen as a ductility exhaustion process. It can be divided into two parts: cyclic creep and static creep. Specifically, cyclic creep generates ratcheting strain causing fatigue damage and static creep causes creep strain leading to creep damage due to static tensile load. However, no matter how drastic the interaction between cyclic creep and static creep is, the a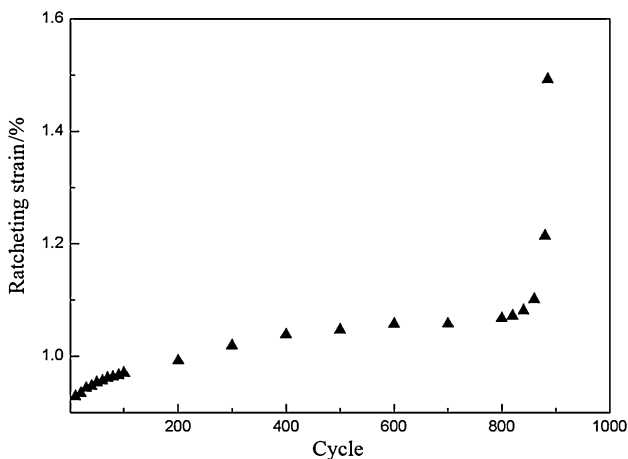ccumulated plastic strain is the coupling of fatigue damage and creep damage. Therefore, the change in accumulated plastic strain can also be used to describe the overall fatigue–creep damage.

5 Damage model identification

Figure 7 presents the fatigue damage evolution of AISI H13 hot tool steel. Figure 8 shows the experiment results of – 500–1500 MPa in stress-controlled tests with different holding time (0, 10, 30, 60, 180 and 600 s). Table 2 gives the detailed impulse density (creep period and fatigue part) and damage exponent for both of fatigue and fatigue–creep.

From Table 2, it can be found that damage exponent decreases with the increase of the impulse density. This means that the high external work will drastically lead to internal damage. Also, the impulse density corresponding to fatigue is relatively smaller than that of creep, and it reveals that the material is more sensitive to impulse density of fatigue part. Figure 9 shows the relationship between the damage exponent and impulse density in fatigue tests. The function of fatigue damage exponent can be obtained as follows:

$$1 - \alpha_0 = 4.97 \times 10^{10} \times E_f^{-3.35} \tag{14}$$

where E_f is the fatigue impulse density.

Regardless of what load form it is, material damage level can be described by the damage exponent. This indicates that the damage exponent of fatigue–creep tests can be substituted into Eq. (14). The calculated results can be defined as the equivalent impulse density. After subtracting the impulse density of fatigue part, the remaining is the equivalent fatigue impulse density transformed from the creep part. Table 3 shows the details of equivalent impulse density of fatigue corresponding to that of creep period. Figure 10 shows detailed fitting curves of equivalent fatigue impulse density and creep impulse density. Therefore, the damage evolution function of AISI H13 at 500 °C can be obtained:

$$D_N = 1 - (1 - D_0)\left(1 - \frac{N}{N_f}\right)^{4.97 \cdot 10^{10} \cdot \left(E_f^{eq}\right)^{-3.35}} \tag{15}$$

$$E_f^{eq} = \frac{(\sigma_{max}^2 + \sigma_{min}^2) \cdot T_0}{\sigma_{max} - \sigma_{min}} + 41.6 \cdot (\sigma_{max} \cdot T_h)^{0.208} \quad \sigma_{min} \leq 0 \tag{16}$$

$$E_f^{eq} = \frac{(\sigma_{max} + \sigma_{min}) \cdot T_0}{2} + 41.6 \cdot (\sigma_{max} \cdot T_h)^{0.208} \quad \sigma_{min} > 0 \tag{17}$$

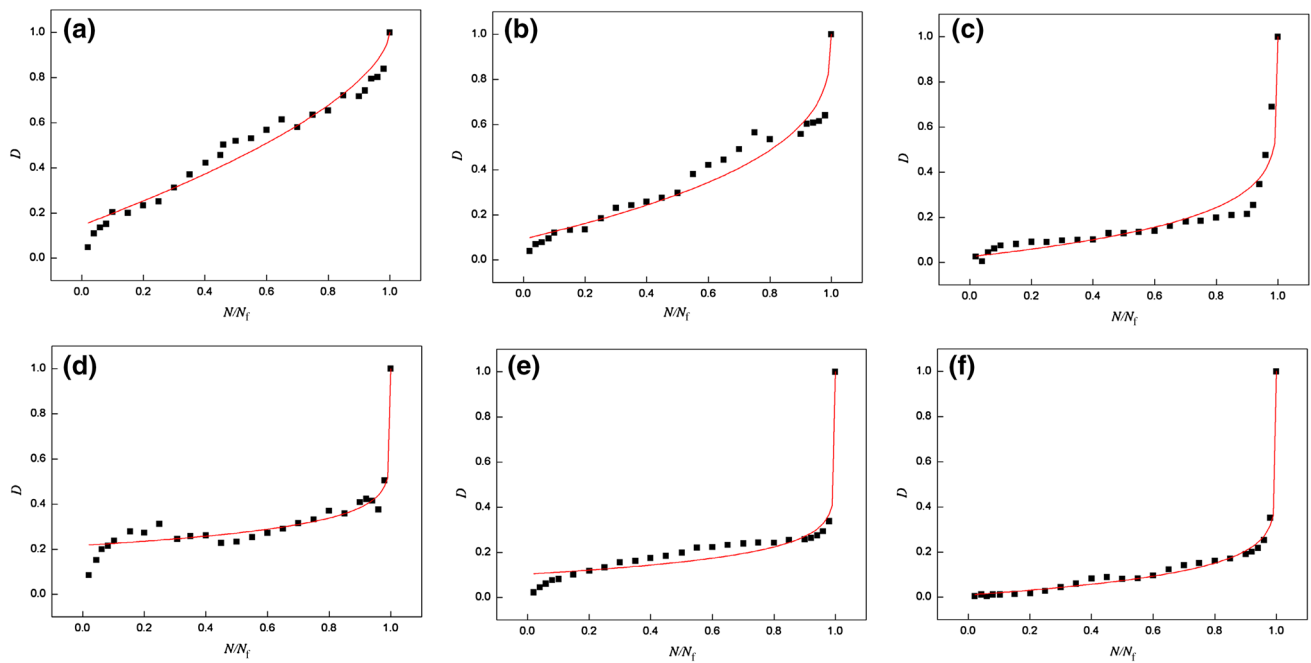where E_f^{eq} is the equivalent fatigue impulse density.

Fig. 6 Ratcheting strain evolution under cycle load of − 800 to 1600 MPa

Fig. 7 Fatigue damage evolution of AISI H13 hot work tool steel under various loads. **a** (− 300)–1300 MPa; **b** (− 400)–1400 MPa; **c** (− 500)–1500 MPa; **d** (− 600)–1600 MPa; **e** (− 800)–1800 MPa; **f** (− 1000)–1300 MPa
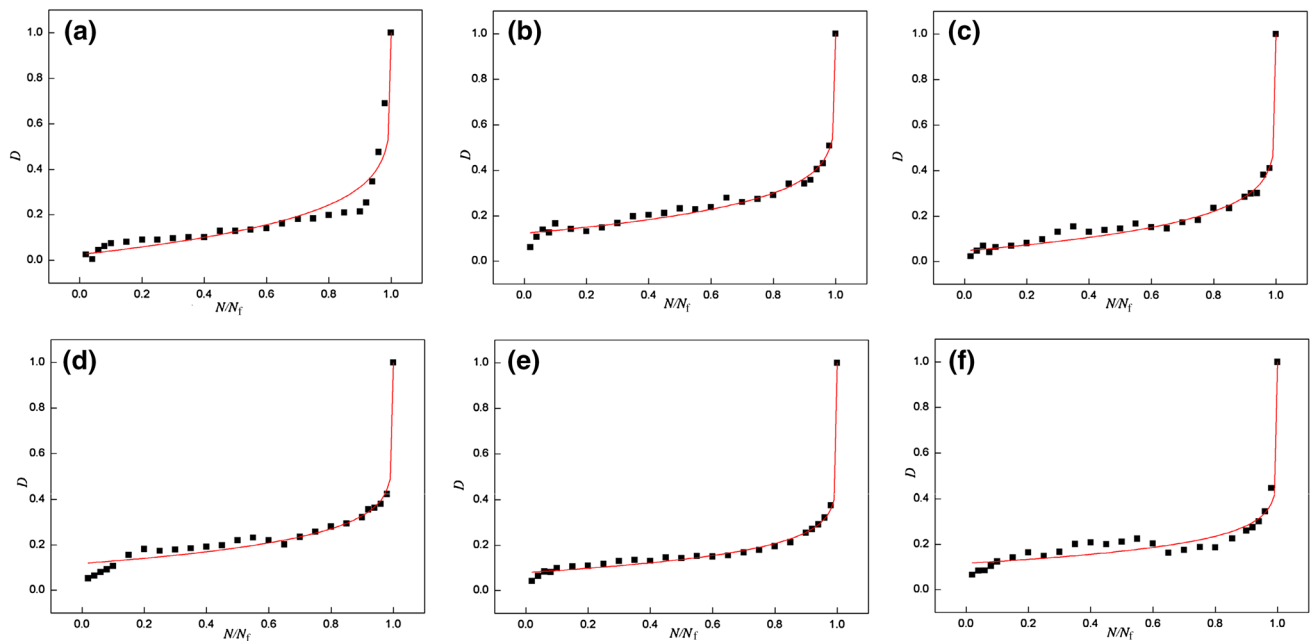

Fig. 8 Damage evolution of − 500–1500 MPa in stress-controlled tests with different holding time. **a** 0 s; **b** 10 s; **c** 30 s; **d** 60 s; **e** 180 s; **f** 600 s

6 Conclusions

1. Creep damage weakens the grain boundary, thus resulting in clearer fatigue striations and more secondary crack. This phenomenon well interprets the damage mechanism of fatigue–creep interaction.

2. The accumulated plastic strain per fatigue–creep cycle is chosen as description of fatigue–creep damage,

Table 2 Details of impulse density and damage exponent

| No.	$\Delta\sigma$/MPa	Holding time/s	Impulse density (fatigue part)/(MPa s)	Impulse density (creep part)/(MPa s)	Damage exponent
1	(-300)–1300	0	1.78×10^3	0	0.606
2	(-400)–1400	0	2.12×10^3	0	0.364
3	(-500)–1500	0	2.50×10^3	0	0.157
4	(-600)–1600	0	2.92×10^3	0	0.104
5	(-800)–1600	0	3.20×10^3	0	0.089
6	(-1000)–1600	0	3.56×10^3	0	0.096
7	(-500)–1500	10	2.50×10^3	1.50×10^4	0.140
8	(-500)–1500	30	2.50×10^3	4.50×10^4	0.124
9	(-500)–1500	60	2.50×10^3	9.00×10^4	0.118
10	(-500)–1500	180	2.50×10^3	2.70×10^5	0.092
11	(-500)–1500	600	2.50×10^3	9.00×10^5	0.088
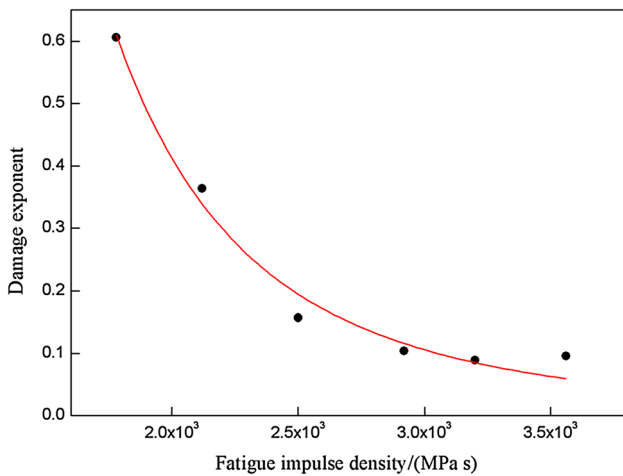
Fig. 9 Relationship between damage exponent and impulse density in fatigue tests

Fig. 10 Fitting curves of equivalent fatigue impulse density and creep impulse density

Table 3 Details of equivalent fatigue impulse density and creep impulse density

No.	Damage exponent	Equivalent fatigue impulse density/(MPa s)	Creep impulse density/(MPa s)
7	0.140	292	1.50×10^4
8	0.124	395	4.50×10^4
9	0.118	438	9.00×10^4
10	0.092	604	2.70×10^5
11	0.088	707	9.00×10^5

which makes the simulation of damage evolution more reasonable and acceptable.

3. By transforming creep impulse density into fatigue impulse density, an equivalent fatigue impulse density was proposed and it can describe the fatigue–creep
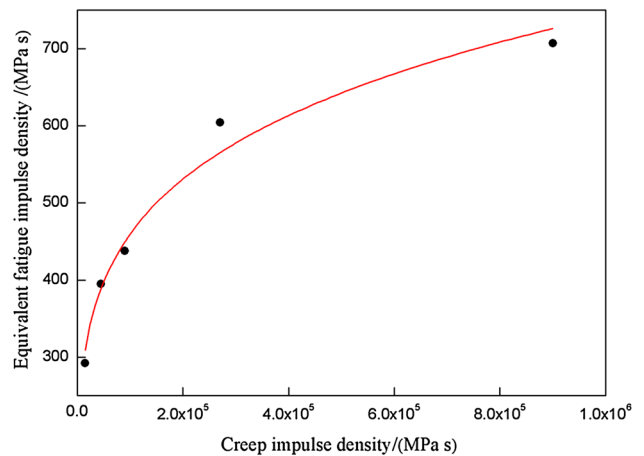
damage evolution of AISI H13 hot work tool steel effectively.

References

[1] E. Olberg, F.D. Jones, Machinery's handbook, Industrial Press Inc., New York, 2001.
[2] A.F.M. Arif, A.K. Sheikh, S.Z. Qamar, J. Mater. Process. Technol. 134 (2003) 318–328.
[3] A.F. Arif, A.K. Sheikh, S.Z. Qamar, K.M. Al-Fuhaid, in: Int. Conf. on Production Res., Prague, 2001, pp. 6–13.
[4] B. Reggiani, L. Donat, J. Zhou, L. Tomesani, J. Mater. Process. Technol. 210 (2010) 1613–1623.
[5] L. Donati, L. Tomesani, J. Mater. Process. Technol. 164–165 (2005) 1025–1031.
[6] S.N. Ab Rahim, M.A. Lajis, S. Ariffin, Procedia CIRP 26 (2015) 761–766.
[7] R. Rodríguez-Baracaldo, J.A. Benito, E.S. Puchi-Cabrera, M.H. Staia, Wear 262 (2007) 380–389.
[8] M. Koneshlou, K.M. Asl, F. Khomamizadeh, Cryogenics 51 (2011) 55–61.

[9] G. Castro, A. Fernández-Vicente, J. Cid, Wear 263 (2007) 1375–1385.

[10] M. Kchaou, R. Elleuch, Y. Desplanques, X. Boidin, G. Degallaix, Eng. Fail. Anal. 17 (2010) 403–415.

[11] J. Li, Y. Shi, X. Wu, Fatigue Fract. Engng. Mater. Struct. 41 (2018) 1260–1274.

[12] G. Telasang, J.D. Majumdar, G. Padmanabham, I. Manna, Surf. Coat. Technol. 261 (2015) 69–78.

[13] Z.X. Jia, Y.W. Liu, J.Q. Li, L.J. Liu, H.L. Li, Int. J. Fatigue 78 (2015) 61–71.

[14] Z.C. Fan, X.D. Chen, L. Chen, J.L. Jiang, Int. J. Press. Vessels Pip. 86 (2009) 628–632.

[15] J.L. Chaboche, Nucl. Eng. Des. 105 (1987) 19–33.

[16] Y.Q. Wang, W.Q. Du, Y.X. Luo, J. Mater. Res. 32 (2017) 1–9.

[17] D. Krajcinovic, J. Lemaitre, Continuum damage mechanics theory and application, Springer Vienna, New York, 1987.

[18] X.H. Yang, N. Li, Z.H. Jin, T.J. Wang, Int. J. Fatigue 19 (1997) 687–692.

[19] S. Tian, M. Fu, C.R. Wang, G.Q. Zhang, Q.Y. Meng, J. Iron Steel Res. Int. 22 (2015) 330–336.

[20] H.Y. Qin, G. Chen, Q. Zhu, C.J. Wang, P. Zhang, J. Iron Steel Res. Int. 22 (2015) 551–556.

[21] Z. Zhang, Z.F. Hu, L.K. Fan, B. Wang, J. Iron Steel Res. Int. 22 (2015) 534–542.

[22] C.Y. Zhang, R.B. Gou, M. Yu, Y.J. Zhang, Y.H. Qiao, S.P. Fang, J. Iron Steel Res. Int. 24 (2017) 214–221.

[23] X.L. Yan, X.C. Zhang, S.T. Tu, S.L. Mannan, F.Z. Xuan, Y.C. Lin, Int. J. Press. Vessels Pip. 126–127 (2015) 17–28.

[24] J. Goodman, Mechanics applied to engineering, Longmans, London, 1941.

[25] Ö. Karakas, Int. J. Fatigue 49 (2013) 1–17.

[26] G.D. Zhang, Y.F. Zhao, F. Xue, J. Mei, Z.X. Wang, C.Y. Zhou, L. Zhang, Nucl. Eng. Des. 241 (2011) 4856–4861.

[27] Y.N. Fan, H.J. Shi, K. Tokuda, Mater. Sci. Eng. A 625 (2015) 205–212.

[28] S.P. Zhu, H.Z. Huang, Y.F. Li, L.P. He, Int. J. Damage Mech. 21 (2012) 1076–1099.

[29] D.M. Ji, M.H.H. Shen, D.X. Wang, J.X. Ren, J. Mater. Eng. Perform. 24 (2015) 194–201.

[30] J. Lemaitre, J. Dufailly, Eng. Fract. Mech. 28 (1987) 643–661.

[31] C. Gaudin, X. Feaugas, Acta Mater. 52 (2004) 3097–3110.

[32] C.B. Lim, K.S. Kim, J.B. Seong, Int. J. Fatigue 31 (2009) 501–507.